A numeric evaluation of attenuation from ambient noise correlation functions

Jesse F. Lawrence[1*], Marine Denolle[1], Kevin J. Seats[1], Germán A. Prieto[2]

[1]Geophysics Department, Stanford University, Stanford, California, 94306, USA

[2]Departamento de Física, Universidad de los Andes, AA 4976, Bogotá, Colombia

* to whom correspondence should be made: jflawrence@stanford.edu

Under appropriate conditions it is well known that ambient noise correlation functions (NCFs) contain interstation accurate and repeatable travel-time information. However, the interpretation of NCF amplitudes, which are likely affected by seismic attenuation, scattering, focusing, source intensity, and geometrical spreading, is highly debated. In this study, NCFs are shown to preserve accurate geometrical spreading and attenuation decay information for a large suite of synthetic simulations computed with a laterally homogeneous model and the coherency NCF method. Important conditions for recovering accurate phase velocity and attenuation coefficients following *Prieto et al.* [2009] include 1) >3 noise sources within each time window, 2) good azimuth distribution of noise sources outside the receiver array, 3) enough time windows stacked to create the NCFs, and 4) seismic arrays with many receiver-receiver azimuths and distances. For well-constructed synthetic NCFs, the real portion of the coherency matches a Bessel function exponentially decayed by an attenuation coefficient. When a single noise source per time window is chosen, the numerical result is shown to match the single-source field analytic approximation (no attenuation). We also demonstrate that estimated attenuation coefficients are sensitive to attenuation beneath the receiver array, and not sensitive to attenuation between the sources and receivers.

Introduction:

Recent developments in seismology make use of the ambient seismic field to extract properties of the Earth of particular interest. The cross-correlation of the noise continuously recorded at two stations, which we refer as the noise correlation function (NCF), has been widely studied for its extensive range of applications [e.g., *Shapiro et al*., 2005; *Sabra et al*., 2005*a,b*; *Yao et al*., 2006; *Zheng et al*., 2008, *Prieto et al*, 2011, *Sabra et al*., 2009, *de Ridder et al*., 2011]. Repetitively stacking cross-correlations of short time series of seismic noise yields NCFs that are remarkably similar to the Green's function between the two receivers [e.g., *Weaver and Lobkis*, 2001, 2004; *Derode et al*., 2003*a,b*; *Shapiro and Campillo*, 2004; *Wapenaar* 2004, 2006; *Sánchez-Sesma and Campillo*, 2006]. To extract such properties of the Earth, traditional approaches in seismology rely on earthquake records and would, consequently, depend on the source occurring at particular locations while the array is recording. This powerful new technique is free from such constraints since the ambient seismic field is continuously recorded at any location. Among the wide range of applications that results from such a technique, researchers have been able to produce higher resolution images of the crustal and upper mantle structure than with traditional approaches [e.g., *Shapiro et al.,* 2005*; Sabra et al.,* 2005b; *Yao et al.,* 2006; *Lin et al*., 2008; *Gudmundsson et al*., 2008; *Yao and van der Hilst*, 2009; *Stehly et al*., 2009].

The ambient seismic field [*Peterson*, 1980; *Peterson*, 1993] may be excited by earthquakes, micro-earthquakes, waves crashing on the shores, or ocean swells coupling energy to the deep oceanic sea floor [e.g., *Longuet-Higgins*, 1950, *Hasselmann*, 1963; *Tanimoto et al*., 1998; *Rhie and Romanowicz*, 2004,2006; *Shapiro et al*., 2006; *Kedar et al*., 2008; *Tanimoto*, 2007; *Zheng et al*., 2008; *Landés et al*., 2010; *Ardhuin et al*., 2011]. Various processes that generate the ambient seismic field are thought to contribute to specific frequency bands. At short periods, [*Longuet-Higgins*, 1950] pioneering work suggests that the interaction of the oceanic waves with the shallow sea floor forms the first microseism peak (10-20s) and the interference of those waves with their reflection forms the second microseism peak (5-10s) even in the deep oceans. At longer periods, interactions between the oceanic swell and the deeper sea floor may generate the "hum" [e.g., *Suda et al*., 1998; *Tanimoto et al.*, 2006; *Rhie and Romanowicz*, 2004,2006].

For studies imaging the crust and upper mantle with the ambient seismic field at regional [e.g., *Gudmonsson et al*., 2008] or continental scale [e.g., *Lin et al*., 2008; *Bensen et al*., 2008], the period band of focus is between 5 and 40 s, but can be extended up to 120 s in some cases [*Lin et al*., 2006]. The ambient seismic field is well distributed and has the highest energy within the microseism peaks, which makes the NCFs highly accurate and repeatable at those periods. NCFs associated with short receiver separation often contain higher signal-to-noise ratios at shorter periods [e.g., *Young et al*., 2011] than NCFs associated with large receiver separation [e.g., *Bensen et al*., 2008]. This observation is consistent with the convergence of correlation towards the Green's function as $\sqrt{r_{xy}k}$ (where k is wavenumber and $r_{\mathbf{xy}}$ is the receiver separation [*Sabra et al.,* 2005*a*; *Larose* 2008; *Weaver and Lobkis* 2005]). This trend may be due to several factors including 1) incoherency caused by differences in the ambient noise near each receiver, 2) incoherency caused by small-scale scattering or 3D heterogeneity, and 3) intrinsic attenuation decreasing amplitudes of short-period waves more than long-period waves. Note that convergence towards a stable NCF is much faster for short-windowed simple coherency NCFs [*Seats et al.,* 2012] as compared to the typical long-duration one-bit normalization or running-normalization NCFs [e.g., *Bensen et al*., 2008] used in many studies.

Several authors have observed that NCF amplitudes preserve relative amplitudes associated with the Green's function between two receivers [*Weaver and Lobkis*, 2001; *Larose et al*., 2005; *Prieto and Beroza*, 2008; *Colin de Verdière*, 2006*a,b*; *Prieto et al.,* 2009; *Colin de Verdière*, 2009; *Cupillard and Capdeville*, 2010; *Harmon et al.*, 2010; *Lawrence and Prieto*, 2011; *Prieto et al*., 2011]. As discussed below, there is a clearly formulated mathematical understanding of the decrease in amplitude with distance due to purely elastic geometrical spreading, which can be modeled as a first order Bessel function for cylindrically expanding Rayleigh waves [e.g., *Sánchez-Sesma and Campillo*, 2006; *Ekström et al*., 2009; *Prieto et al*., 2011]. There are variant forms [e.g., *Colin de Verdière*, 2006*a,b*] depending on assumptions of the medium, wave propagation formulation, and chosen source-receiver geometries.

Whether or not the attenuation can be extracted from the NCF technique is still controversial [e.g., *Harmon et al*., 2010; *Tsai*, 2011; *Weaver*, 2011]. *Prieto et al*., [2009] demonstrated that, using the spatial autocorrelation (SPAC) method [e.g., *Aki*, 1957], the decay of amplitudes with increased station separation was greater than expected for a laterally homogeneous and purely elastic medium (e.g., the first order Bessel Function from *Sánchez-Sesma and Campillo* [2006]). From a one-dimensional medium [*Prieto et al*., 2009] to a regionalized laterally varying medium [*Lawrence and Prieto*, 2011], this amplitude decay can be modeled with an attenuation coefficient for which the interpretation as intrinsic attenuation concurs and is validated with observations made with other earthquake-based techniques. The method provides geophysically reasonable results at small [*Weemstra et al*., 2011*a,b*] and large [*Lawrence and Prieto*, 2011] scales. *Lin et al*. [2011] confirmed that amplitude decay as a function of receiver separation for NCFs conforms to an increased decay expected in an attenuating medium [see also *Cupillard and Capdeville*, 2010].

Prior numerical, analytical and observational studies [*Colin de Verdière*, 2006*a,b*; *Colin de Verdière*, 2009; *Cupillard and Capdeville*, 2010; *Harmon et al*., 2010; *Tsai* 2011; *Weaver*, 2011] disagree on whether and how NCF amplitudes depend on intrinsic attenuation and source distribution (or source intensity). *Colin de Verdiere* [2006*a*; 2009] shows that the NCF is sensitive to the attenuation of the medium for both homogeneous distribution of sources or when equipartition is fulfilled at the boundaries of the region of interest [see also *Goudard et al.*, 2008]. *Weaver* [2011] and *Tsai* [2011] suggest that NCF amplitudes highly depend on noise source distribution, but interestingly disagree for uniformly distributed sources., *Weaver* [2012] suggesting that no attenuation dependence is observed while *Tsai* [2011] shows the expected exponential decay for surface waves. A global-scale numerical simulation [*Cupillard and Cadeville*, 2010] corroborated that for uniformly distributed noise sources, NCF amplitude decay depends on the attenuation of the medium.

Much of the debate regarding the recovery of attenuation from NCFs may largely depend on the differing assumptions made regarding the equipartition of the ambient source field. We stress that the Earth's ambient source field is not equipartitioned. The source distribution appears to vary spatially and temporally, depending on seasonal effects, proximity to the coast, and frequency band. Many studies [e.g., *Schulte-Pelkum et al*., 2004; *Stehly et al.,* 2006; *Chevrot et al*., 2007] have found that the second microseismic band (5-10s) consistently propagates from a direction consistent with the nearby local coast line, while the primary microseismic band (10-20s) changes corresponding to the seasonal weather patterns. More recent back projected ambient field source studies [e.g., *Aster et al*., 2008; *Yang and Ritzwoller*, 2008; *Gerstoft et al*., 2008; *Kedar et al*., 2008; *Koper et al.*, 2009; *Stutzmann et al*., 2009; *Zhang et al*., 2009; *Ardhuin et al*., 2011] temporally correlate high amplitude ambient fields with wave-height images and seasonal weather patterns.

Because the source field is not equipartitioned, the assumption of equipartition requires that the time-averaging of correlations for many amplitude-normalized records of waves from distinct ambient sources is equal to the integration over all source angles with respect to the origin. Each additional time window contributes to a NCF by providing a better distribution of noise sources. Normalization of the ambient field is thought to help with normalizing the source terms such that the recorded ambient wave field approximates equipartition. In practice, normalization is applied to the recorded waveforms, not the distinct waves propagating from each source. The recorded waveform can be considered as a summation of displacements measured after geometrical spreading and attenuation from a diverse source distribution. With multiple sources per time window (each having different amplitudes and distances), the question remains whether equipartition is sufficiently approximated for attenuation recovery from the NCF

Despite concerns of equipartition, attenuation coefficients measured with the method of *Prieto et al.* [2009] are realistic and consistent with geologic interpretation [*Prieto et al*., 2009, *Lawrence and Prieto*, 2011, *Prieto et al*., 2011, *Weemstra*, 2012]. Perhaps the process of averaging NCFs across an array (as in *Prieto et al.* [2011]) with many receiver-receiver azimuths artificially reduces the effects of a non-uniform source distribution. Because the method of *Prieto et al.* [2009] yields reasonable attenuation values consistent with earthquake-based methods and geologic structures, we prefer to adopt the assumptions necessary for real data rather than choosing from one of several formulations adopted by prior analytical and numerical studies.

We present here an alternate mathematical formulation of the NCFs from prior studies [e.g., *Sánchez-Sesma and Campillo* [2006]; *Colin de Verdière*, 2006*a,b*; *Colin de Verdière*, 2009; *Tsai* 2011; *Weaver*, 2011]. The theoretical framework is evaluated within various common assumptions (e.g., pure elastic medium and equipartitioning of ambient noise source energy). In this work we evaluate the impact of the noise source and receiver distribution by numerically demonstrating that synthetic NCF amplitudes are consistent with the expected results from *Prieto et al*. [2009]. Our results suggest that in contrast to some of the references above, after azimuthal averaging, we recover accurate attenuation for a wide range of source distributions, but also define the range within which we do not.

We first introduce an analytical solution for the elastic and anelastic eigenproblem of cylindrically expanding waves from arbitrary sources through a laterally homogeneous medium. We describe the effect of various simplifying assumptions on the amplitude recovered from synthetic NCFs. In particular , we focus on the assumption of an equipartitioned ambient source field versus the approximation of an equipartitioned ambient wave field. Given the discrepancies between differing assumptions, we proceed with a numerical approximation to calculate NCFs for a suite of scenarios. We then present the results using as input data the model of *Prieto et al.* [2009] and test different source distributions. We test furthermore whether the estimated attenuation coefficients are sensitive to the region within the receiver array or not. Finally, we discuss the results and draw some conclusions.

Analytical Formulations and Assumptions:

Realistic ambient seismic noise records can be considered as the sum of all wavefields propagating from all sources to the receiver. For a single point source F located at **s**, the displacement u, recorded at location **x** is given by:

$$u_x(\mathbf{s},\omega) = F(\mathbf{s},\omega)e^{i\omega t}e^{-ikr_{\mathbf{sx}}}e^{-\alpha(\omega)r_{\mathbf{sx}}}\Big/\sqrt{r_{\mathbf{sx}}}\,, \qquad 1$$

where ω is the frequency, k is the wavenumber, t is the source time [*Sánchez-Sesma and Campillo,* 2006], $\alpha(\omega)$ is the frequency-dependent attenuation coefficient, and $r_{\mathbf{sx}}$ is the source to receiver separation. This is a far-field approximation to the cylindrically expanding wave eigenproblem, where we have incorporated an attenuation term and a geometrical spreading term for a cylindrically expanding point source, $1\big/\sqrt{r_{\mathbf{sx}}}$. As with

Prieto et al. [2009], we consider only the vertical component of the propagating Rayleigh waves.

From equation 1, there are a series of simplifying assumptions that can yield different interpretations regarding the effect of intrinsic attenuation on the NCF. The most common assumption, yet not met in practice, is that the sum of the correlations (or cross spectra) of each source is approximately equal to the correlation of the sum of all sources. For example, following *Sánchez-Sesma and Campillo* [2006], the cross spectrum of data records for a single source recorded at two stations **x** and **y**, where **y** is the origin, gives

$$C_{\mathbf{xy}} = u_{\mathbf{x}}(\mathbf{s},\omega)u_{\mathbf{y}}^{*}(\mathbf{s},\omega) = \left|F(\mathbf{s},\omega)\right|^{2} e^{-ik\zeta_{\mathrm{y}}\cos[\varphi-\theta]} e^{-\alpha(\omega)r_{\mathrm{sx}}} e^{-\alpha(\omega)r_{\mathrm{sy}}} \Big/ \sqrt{r_{\mathbf{sx}}}\sqrt{r_{\mathbf{sy}}}\,, \qquad 2$$

where * indicates complex conjugate, $r_{\mathbf{xy}}$ is the receiver separation, θ is the azimuth from receiver **y** to the source, ψ is the angle from receiver **x** to the source, and $e^{-ikr_{\mathrm{sx}}}e^{ikr_{\mathrm{sy}}} = e^{-ik\left(r_{\mathrm{sy}}+r_{\mathrm{xy}}\cos[\varphi-\theta]\right)}e^{ikr_{\mathrm{sy}}} = e^{-ikr_{\mathrm{xy}}\cos[\varphi-\theta]}$ (if **y** = 0). The NCF technique calls for averaging the correlations (or cross spectra) over many time windows in order to azimuthally average many distinct sources. This leads to a temporal/azimuthal averaging similar to

$$\left\langle C_{\mathbf{xy}}\right\rangle = \left\langle u_{\mathbf{x}}(\mathbf{s},\omega)u_{\mathbf{y}}^{*}(\mathbf{s},\omega)\right\rangle = \frac{1}{2\pi}\iint \frac{\left|F(\mathbf{s},\omega)\right|^{2}}{\sqrt{r_{\mathbf{sx}}}\sqrt{r_{\mathbf{sy}}}} e^{-ikr_{\mathrm{xy}}\cos[\varphi-\theta]} e^{-\alpha(\omega)r_{\mathrm{sx}}} e^{-\alpha(\omega)r_{\mathrm{sy}}}\, dr d\theta\,, \qquad 3$$

where $\langle\rangle$ indicates the ensemble average over time.

With several simple assumptions, we can recover the solution of *Sánchez-Sesma and Campillo* [2006] from our chosen formation (equation 1). These assumptions include 1) equipartitioning of the source field (i.e., $\left|F(\mathbf{s},\omega)\right|$ and $\sqrt{r_{\mathbf{sx}}}$ are constant for all sources), 2) the far field approximation ($r_{\mathbf{xy}} << r_{\mathbf{sx}} \approx r_{\mathbf{sy}}$), and 3) a purely elastic medium (α=0), equation 3 becomes:

$$\left\langle C_{\mathrm{xy}}\right\rangle = \left\langle u_{\mathrm{x}}(\mathbf{s},\omega)u_{\mathrm{y}}^{*}(\mathbf{s},\omega)\right\rangle = \frac{\left|\bar{F}(\mathbf{s},\omega)\right|^{2}}{2\pi\bar{r}}\iint e^{-ikr_{\mathrm{xy}}\cos[\varphi-\theta]}\, dr d\theta\,, \qquad 4$$

where, $\bar{F}$ is the constant source, and $\bar{r}$ is the constant source-receiver separation. The assumption of $r_{\mathbf{sx}} \approx r_{\mathbf{sy}}$ likely introduces some degree of inaccuracy – but is necessary for simplifying equation 4 to a manageable analytic solution that converges to the expected Green's function form. With the above assumptions, equation 4 simplifies to

$$\left\langle C_{\mathbf{xy}} \right\rangle = \frac{\left|\bar{F}(\mathbf{s},\omega)\right|^2}{2\pi\bar{r}} J_0(k\bar{r}) \propto J_0\big(\omega\bar{r}/C(\omega)\big), \qquad 5$$

where J_0 is the Bessel function, and C is the phase velocity of the medium. The Bessel function formulation is ideal because it is the imaginary portion of the inter-station elastic Green's function [e.g., *Sánchez-Sesma and Campillo*, 2006] and provides a direct link between the Green's function and phase velocity tomography results [*Ekström et al.,* 2009].

In order to measure appropriate amplitudes for attenuation analysis, *Prieto et al.* [2009] computed the time-averaged white-balanced coherence,

$$\gamma_{\mathbf{xy}}(\omega) = \left\langle \frac{u_{\mathbf{x}}(\mathbf{s},\omega)u_{\mathbf{y}}^{*}(\mathbf{s},\omega)}{\left\{\left|u_{\mathbf{x}}(\mathbf{s},\omega)\right|\right\}\left\{\left|u_{\mathbf{y}}(\mathbf{s},\omega)\right|\right\}} \right\rangle, \qquad 6$$

where {} indicates the spectral average over ~20 frequency points, || is the absolute value, and ⟨⟩ is the time averaged ensemble. The coherency is frequency normalized for the whole displacement record, not on a source-by-source basis (i.e., equipartition is only approximated, not necessarily achieved). Nevertheless, *Prieto et al.* [2009] empirically demonstrated that the real portion of time-averaged coherence resembles a Bessel function (equation 5) modified by an attenuation term,

$$\mathrm{Re}\left[\gamma_{\mathbf{xy}}(\omega)\right] \approx J_0\big(\omega r_{\mathbf{xy}}/C(\omega)\big)e^{-\alpha(\omega)r_{\mathbf{xy}}}. \qquad 7$$

Prieto et al. [2009] use raw signal and do not pre-process the data with the typical approaches of one-bit or running normalizations [e.g., *Bensen et al*., 2007]. *Seats et al.* [2012] demonstrated that applying equation 6 with short duration time series (30-60min instead of day-long time series) and overlapping time windows (Welch's Method, Welch, [1969]) provides faster convergence to stable and robust NCFs than with other pre-processing techniques. Because the amplitudes do not appear to be well preserved with just the cross-spectrum, long-time windowed data, nor pre-normalized data, we initially set out to solve for a solution of 6 that yields equation 7.

Unfortunately, obtaining equation 7 analytically from coherency is not straightforward, if variables such as source amplitudes $F(\mathbf{s},\omega)$, source distances ($r_{\mathbf{sx}}$, $r_{\mathbf{sy}}$)

and seismic attenuation are included (e.g., equations 12, 16, and 18 from *Tsai* [2011] or equation 9 from [*Colin de Verdière*, 2006*a*]). Given specific cases, one can make approximations to simplify equation 2. However, most tend to collapse to a form similar to equation 3 (e.g., equation 23 in [*Tsai*, 2011], sometimes with an added term or two). The resulting expressions are strongly case-dependent on factors such as the source distribution and source-receiver geometry [*Tsai* 2011] or source spectrum [*Colin de Verdière*, 2006].

We state that applying equation 3 or similar expressions is inherently flawed. The operations of integration and multiplication are not permutable, unless the variables are constant with respect to integration. For elastic plane wave sources this may be a reasonable assumption. In reality, the geometrical spreading ($r_{\mathbf{sx}}^{-0.5}$) and attenuation ($e^{-\alpha(\omega)r_{\mathbf{sx}}}$) term negate this assumption unless all $r_{\mathbf{sx}}$ are equal and constant (a physical impossibility for distinct receiver locations). Unless the source field $F(\mathbf{s},\omega)$ exactly counters the effect of the attenuation and geometrical spreading for a receiver pair ($\mathbf{x}$,$\mathbf{y}$), equipartition for a set of point sources cannot be assumed.

Colin de Verdière [2008] took a different route to formulate the correlation, starting from a different set of assumptions and obtained a different solution that accounts for amplitude decay (geometrical spreading and attenuation). Unfortunately, the set of initial conditions are not tenable for application to real data, ("homogeneous white noise"). If whitening the displacement records for coherency were equivalent to the cross-spectrum of records of waves propagating from "homogeneous white noise", then the attenuation should augment NCF amplitudes by $e^{-\alpha(\omega)r_{\mathbf{xy}}}/4\alpha(\omega)$. This suggests that the NCF amplitudes for an attenuating medium should be modified by $\frac{1}{4\alpha(\omega)}$ relative to the observations of *Prieto et al.* [2009]. This yields a two order of magnitude amplitude discrepancy between theory and observation (assuming attenuation coefficients in the range of 10^{-3} to 10^{-2} [e.g., *Yang and Forsyth*, 2008]). The expected discrepancy is not observed.

Given the agreement between NCF and earthquake attenuation measurements [*Yang and Forsyth*, 2008] we choose to continue with coherency over cross spectrum with an assumed ambient source field equipartition. We expand the cylindrically expanding elastic and anelastic eigenproblem solution for a laterally homogeneous medium (equation 1) to account for all sources contributing to a displacement record at a single station,

$$u_{\mathbf{x}}(\omega) = \iint \frac{F(\mathbf{s},\omega)}{\sqrt{r_{\mathbf{sx}}}} e^{i\omega t} e^{-ikr_{\mathbf{sx}}} e^{-\alpha(\omega) r_{\mathbf{sx}}} dr d\theta \,. \qquad 8$$

The cross-spectrum for a receiver pair (**x**,**y**) for many sources becomes

$$u_{\mathbf{x}}(\omega) u_{\mathbf{y}}^{*}(\omega) = \iint \frac{F(\mathbf{s},\omega)}{\sqrt{r_{\mathbf{sx}}}} e^{i\omega t} e^{-ikr_{\mathbf{sx}}} e^{-\alpha(\omega) r_{\mathbf{sx}}} dr d\theta \iint \frac{F(\mathbf{s},\omega)}{\sqrt{r_{\mathbf{sy}}}} e^{-i\omega t} e^{ikr_{\mathbf{sy}}} e^{-\alpha(\omega) r_{\mathbf{sy}}} dr d\theta \,. \qquad 9$$

Equation 9 distinctly differs from equation 3 or 4. The coherency presented in equation 6 is then given by

$$\gamma_{\mathbf{xy}}(\omega) = \left\langle \frac{\iint F(\mathbf{s},\omega) e^{i\omega t} e^{-ikr_{\mathbf{sx}}} e^{-\alpha(\omega) r_{\mathbf{sx}}} \big/ \sqrt{r_{\mathbf{sx}}}\, dr d\theta \iint F(\mathbf{s},\omega) e^{-i\omega t} e^{ikr_{\mathbf{sy}}} e^{-\alpha(\omega) r_{\mathbf{sy}}} \big/ \sqrt{r_{\mathbf{sy}}}\, dr d\theta}{\left\{\left| \iint F(\mathbf{s},\omega) e^{i\omega t} e^{-ikr_{\mathbf{sx}}} e^{-\alpha(\omega) r_{\mathbf{sx}}} \big/ \sqrt{r_{\mathbf{sx}}}\, dr d\theta \right|\right\} \left\{\left| \iint F(\mathbf{s},\omega) e^{i\omega t} e^{-ikr_{\mathbf{sy}}} e^{-\alpha(\omega) r_{\mathbf{sy}}} \big/ \sqrt{r_{\mathbf{sy}}}\, dr d\theta \right|\right\}} \right\rangle . \qquad 10$$

From this point, there are several options for simplification of the coherency method used in *Prieto et al*. [2009]. If one takes the analytical path, assumptions need to be made to simplify equation 10. A first approximation is to assume that the source spectrum is white at each source. This reduces equation 10 to

$$\gamma_{\mathbf{xy}}(\omega) = \left\langle \frac{\iint e^{-ikr_{\mathbf{sx}}} e^{-\alpha(\omega) r_{\mathbf{sx}}} \big/ \sqrt{r_{\mathbf{sx}}}\, dr d\theta \iint e^{ikr_{\mathbf{sy}}} e^{-\alpha(\omega) r_{\mathbf{sy}}} \big/ \sqrt{r_{\mathbf{sy}}}\, dr d\theta}{\left\{\left| \iint e^{-ikr_{\mathbf{sx}}} e^{-\alpha(\omega) r_{\mathbf{sx}}} \big/ \sqrt{r_{\mathbf{sx}}}\, dr d\theta \right|\right\} \left\{\left| \iint e^{-ikr_{\mathbf{sy}}} e^{-\alpha(\omega) r_{\mathbf{sy}}} \big/ \sqrt{r_{\mathbf{sy}}}\, dr d\theta \right|\right\}} \right\rangle . \qquad 11$$

Let's now assume that one single source dominates each time series. In this case, the integrations in equation 11 disappear and leave the coherency to be

$$\gamma_{\mathbf{xy}}(\omega) = \left\langle \frac{e^{-ikr_{\mathbf{sx}}} e^{-\alpha(\omega) r_{\mathbf{sx}}} \big/ \sqrt{r_{\mathbf{sx}}}\, e^{ikr_{\mathbf{sy}}} e^{-\alpha(\omega) r_{\mathbf{sy}}} \big/ \sqrt{r_{\mathbf{sy}}}}{\left\{\left| e^{-ikr_{\mathbf{sx}}} e^{-\alpha(\omega) r_{\mathbf{sx}}} \big/ \sqrt{r_{\mathbf{sx}}} \right|\right\} \left\{\left| e^{-ikr_{\mathbf{sy}}} e^{-\alpha(\omega) r_{\mathbf{sy}}} \big/ \sqrt{r_{\mathbf{sy}}} \right|\right\}} \right\rangle . \qquad 12$$

If we assume that the derivative of phase velocity, $dC(\omega)/d\omega$, and attenuation, $d\alpha(\omega)/d\omega$ are small, then the average ensemble is approximately value itself, or $z/\{z\}\approx 1$. This further simplify equation 12 to give

$$\gamma_{\mathbf{xy}}(\omega) = \left\langle e^{-ikr_{\mathbf{sx}}} e^{ikr_{\mathbf{sy}}} \right\rangle , \qquad 13$$

which is independent of attenuation and simplifies to the un-attenuated Bessel function (equation 5) [*Weaver*, 2011] under the assumption of an equipartitioned far-field source field (as performed above). This lack of sensitivity to attenuation disagrees with the observations [*Prieto et al.*, 2009; *Lawrence and Prieto*, 2011; *Weemstra et al.*, 2011*a,b*], previous theoretical studies [*Colin de Verdière* 2008, *Tsai* 2011], and numerical analyses [e.g., *Cupillard and Capdeville*, 2010]. Simplifying equation 10 for reasonable expressions requires strong assumptions. In the following we turn to numerical evaluation of the coherency and compute directly a discrete version of equation 10.

Numerical solution:

For numerical calculations, we write equation 10 with a discrete set of sources,

$$\gamma_{\mathbf{xy}}(\omega) = \left\langle \frac{\sum_{j=1}^{N_s} F(\mathbf{s}_j,\omega) e^{i\omega t} e^{-ikr_{\mathbf{s}_j\mathbf{x}}} e^{-\alpha(\omega) r_{\mathbf{s}_j\mathbf{x}}} \Big/ \sqrt{r_{\mathbf{s}_j\mathbf{x}}} \sum_{j=1}^{N_s} F(\mathbf{s}_j,\omega) e^{-i\omega t} e^{ikr_{\mathbf{s}_j\mathbf{y}}} e^{-\alpha(\omega) r_{\mathbf{s}_j\mathbf{y}}} \Big/ \sqrt{r_{\mathbf{s}_j\mathbf{y}}}}{\left\{\left|\sum_{j=1}^{N_s} F(\mathbf{s}_j,\omega) e^{i\omega t} e^{-ikr_{\mathbf{s}_j\mathbf{x}}} e^{-\alpha(\omega) r_{\mathbf{s}_j\mathbf{x}}} \Big/ \sqrt{r_{\mathbf{s}_j\mathbf{x}}}\right|\right\}\left\{\left|\sum_{j=1}^{N_s} F(\mathbf{s}_j,\omega) e^{i\omega t} e^{-ikr_{\mathbf{s}_j\mathbf{y}}} e^{-\alpha(\omega) r_{\mathbf{s}_j\mathbf{y}}} \Big/ \sqrt{r_{\mathbf{s}_j\mathbf{y}}}\right|\right\}} \right\rangle, \qquad 14$$

where N_s is the number of sources. The medium is laterally homogeneous, but we assume Rayleigh-waves phase velocity $C(\omega)=\omega/k$ and attenuation $\alpha(\omega)$ dispersions, as estimated from *Prieto et al.* [2009] for southern California. We explore the source distribution $\mathbf{s}$ and spectra $F(\mathbf{s},\omega)$ to a given receiver geometry $\mathbf{x}$ to estimate the coherency.

To better reflect reality, we need to account for incoherent noise such as site effects, electrical noise, wind, thermal effects, cultural noise, micro-seismicity, and anything that can create vibrations above the sensitivity of one sensor and below the sensitivity of the other. To do so, we add a degree of white noise, n, to each seismogram. We keep the local or incoherent noise constant, and vary the source amplitudes to account for different coherent-signal-to-incoherent-noise ratios.

To validate the technique of *Prieto et al.* [2009], we need to recover from dispersion measurements the phase velocities and attenuation coefficients used to generate the $\mathrm{Re}[\gamma_{\mathbf{xy}}(\omega)]$ values. As in *Prieto et al.* [2009], we average all $\mathrm{Re}[\gamma_{\mathbf{xy}}(\omega)]$ for each station separation, sampled at a 2 km interval, regardless of the array aperture. We then conduct a 3-stage grid search for the appropriate value of phase velocity and attenuation coefficient by minimizing the L1 norm residuals derived from equation 7 at a given frequency. Our analysis is focused on the period band of the microseism ambient field (7 – 24 seconds).

We verify equation 7 by evaluating equation 14 for different source and receiver distributions with sufficient amount of time-windows to stack. We find that equation 7 is not satisfied in the cases where:

- There are not enough sources (azimuthal averaging is not possible).
- The sources are at the center of the receiver array (insufficient azimuthal averaging).
- The incoherent noise is too high.
- There are not enough receivers (poor azimuthal averaging and distance sampling).

Consequently, most successful simulations require a) at least one source per time window (which is reasonable given that the microseism bands appears to be excited at all times), b) that sources have many separate locations, c) at least 100 receivers (previous studies have all used more than 100 receivers), and d) that the coherent signal (far-field sources) be larger than the incoherent signal.

Synthetic Sources:

To reflect a realistic ambient seismic field, we allow the synthetic sources can take a variety of forms, including the ones coming from oceanic waves, wind on mountains, or directly earthquakes, micro-earthquakes, cultural noise. Each source type has its own spatial, temporal and magnitude distribution. We consider linear source arrays for oceanic waves crashing on a local shore and earthquakes along a local fault line. We impose the oceanic sources to be more frequent than the tectonic sources. At a global scale (greater distances), we reasonably assume that the ocean waves on a coast or teleseismic sources at plate boundaries to be circular source arrays. We model the coherent cultural noise as clusters within which the sources are randomly distributed, but periodically triggered. Storm-driven ocean waves coupled to the sea bottom may be viewed as broad areas of randomly distributed sources varying in source amplitude through time. We allow order of magnitudes of amplitude variation for all coastal and tectonic sources.

We impose a scaled delta function for source time functions. We model the sources as a stochastic logarithmic Gutenberg-Richter magnitude frequency relationship [*Gutenberg* *and Richter*, 1954]. While a Gutenberg-Richter relationship may not be exactly accurate for describing all vibrations in the microseism band, we merely suggest that stronger sources are less common than weaker sources [*Ardhuin et al.*, 2011]. Alternate distributions where larger sources are less common (e.g., a truncated Rayleigh distribution to model wave height [*Wilks*, 1995]) tend to yield similar results. We experiment with the number of sources per time window (N_s) that could yield a reasonable theoretical ambient field. We compute the theoretical coherency using a series of spatial source distributions (Figure 1): A) a uniformly random distribution along a circle, B) a uniformly random set of sources along a line, C) a uniformly random source area, D) a uniformly random source shell or ring area.

Receivers:

We use a single uniformly random two-dimensional receiver array defined by two parameters: 1) the receiver length scale ($L_\mathbf{x}$=100km) and 2) the number of receivers (N_x=100). This parameterization gives an average receiver density of one per 18km^2. Using an uneven receiver spacing ensures a better sampling of the distance between 1 and 200km when sampled at a 2km interval (albeit unevenly covered with respect to receiver spacing). Those scales again reflect the ones encountered in regional surface-wave tomography, but this is arbitrary. We stay consistent and keep the array geometry fixed among the simulations.

Generalized Parameterization:

To better understand the scaling and relation between parameters, we non-dimensionalize key parameters. We normalize the source-length scale $L_\mathbf{s}$, and the source-receiver separation $\Delta_\mathbf{sx}$ by the receiver-length scale $L_\mathbf{x}$. We simply have a source distribution wider than the receiver one if $L_\mathrm{s}/L_\mathrm{x}$>1, sources entirely outside of the receiver array if $\Delta_\mathbf{sx}/L_\mathbf{x}$>1**.** The azimuth of the sources relative to the center of the array is greater than 90 degrees if $L_\mathbf{s}/\Delta_\mathbf{sx}$>1.

Another factor to consider is the number of sources, $N_\mathbf{s}$, relative to the magnitude distribution, $M_\mathbf{s}$. The larger the range of source amplitudes used to generate the synthetic spectra, the fewer sources there are that dominate any given seismogram. Consequently the fraction $10^{N_s}/(M_{\mathbf{s}}+1)$ provides a measure of the number of sources contributing to the spectra. Due to geometrical spreading, the range of source-to-receiver distances also plays an important roll in the number of dominant sources: [max($r_{\mathbf{sx}}$)-min($r_{\mathbf{sx}}$)]. We compute time-series of 1800s, as found to be optimal for fastest convergence of the NCF toward the long-term stable NCF [*Seats et al.*, 2012].

Results:

For a given scenario, we generate synthetic ambient noise seismograms, compute the coherencies (in frequency domain) or NCFs (in time domain), stack Re[$\gamma_{\mathbf{xy}}(\omega)$] over the receiver array (to span the range space), estimate phase velocity and attenuation coefficients and finally evaluate the relative fit of equation 7. For clarity, Table 1 describes the parameterizations of various simulations run to test equations 7 and 14.

The synthetic noise seismograms are a good visual control of similarity between the generated noise and the true ambient seismic field. Figure 2 shows examples of the generated ambient seismic field with different noise source distribution and the resulting variability in the signals. Due to the stochastic nature of our source set up, we can describe the statistics related to seismograms, which change as a function of source-receiver geometry and number of sources per time window.

Figure 2 presents example synthetic noise seismograms for the four source distributions illustrated in Figure 1, namely circular, linear, uniform, and uniform shell. We imposed 128 sources per time window (N_s=128) because it provides a reasonable balance between synthetics seismograms with identifiable phases above the noise and those without. With 128 sources per time window, $\Delta_{\mathbf{sx}}$=500, $L_{\mathbf{s}}$=1000, and $L_{\mathbf{x}}$=100, only $14\pm^{9}_{5}$% of the time windows contain events that have a short-term average (STA) over 4s to long-term average (LTA) over 60s ratio (STA/LTA) greater than 2. We find that the number of detectable phases increases ($23\pm^{62}_{9}$%) as N_s decreases ($1<N_s<64$), but only marginally decreases ($10\pm^{7}_{4}$%) as N_s increases ($N_s > 256$).

Figure 3 shows time-domain NCFs for selected receiver pair in one of our simulations with encouraging results. The phase velocity is consistent with the input values and the amplitudes decrease with increasing station separation as expected due to geometrical spreading and attenuation. In this example a uniformly random source location distribution was used leading to symmetric NCFs.

In Figure 4, the real portion of the coherency of our synthetic signals (equation 10) is compared to the theoretical elastic and the attenuated Bessel function. Coherencies qualitatively match the expected Bessel function, but the amplitudes often match the attenuated Bessel function better. In this figure we have used phase velocities and attenuation coefficients from our input model for comparison, but in practice these parameters are not known.

A better demonstration of the technique is to estimate the phase velocity and attenuation coefficients from the synthetic coherencies. We proceed with a 3-stage grid search for phase velocity following *Prieto et al*. [2009] and *Lawrence and Prieto* [2011]. Figure 5 qualitatively illustrates the accuracy of the recovered dispersion and attenuation curves for the periods used in the *Prieto et al.* [2009] and *Lawrence and Prieto* [2011] studies (8-24 s).

Figure 5 confirms that retrieving correct phase velocities is possible for a wide range of source distributions. The estimated attenuation coefficients show a greater percentage of errors compared to our input model than the phase velocities. In particular, most source distributions in these examples do a reasonable job in retrieving the correct attenuation coefficient values (except for the linear array). There is no obvious bias of any particular source distribution over the periods of interest (8-24 seconds).

Discussion:

Our results suggest that it is possible to retrieve accurate attenuation coefficient estimates from NCFs. We test a wide range of source distributions length scales, varying the source-receiver distance (Δ_{sx}) and source lengths (L_s), for a single receiver distribution. The root-mean squared (RMS) misfit between the estimated and known phase velocities and attenuation coefficients provides a quantitative measure of the method's accuracy/precision. In Figure 6, we illustrate the RMS misfits for phase velocity and attenuation coefficient for a series of source distributions. There is a range of length-scales within which our method provides reliable results for each tested source distribution. There are two cases where our approach fails to recover accurate phase velocity and attenuation coefficients.

The first case occurs in scenarios where the sources mostly lie within the receiver array (Δ_{sx}<L_x and L_s<L_x), in the near field. This parameter space (dashed boxes in Figure 6) is known to provide a poor azimuthal source distribution, which is a fundamental assumption for most ambient noise studies. This also appears when the source array dimension L_s equals the source-receiver offset Δ_{sx}. In this case, a significant number of sources are within the receiver array and the near-field sources can dominate over the far-field ones.

The second case in which the NCFs fail to provide accurate phases and amplitudes is when the sources are predominantly at very great distance with respect to the array dimension ($\Delta_{sx} >> L_x$), namely large source-receiver distances. With the fixed magnitude of the incoherent, or local, noise, the signal-to-noise ratio decreases as the distance between sources and receivers increases. Consequently, we generate NCFs with degraded phase and amplitudes. We can prevent this failure to retrieve good estimation of phase velocity and attenuation measurement by increasing the source magnitude (as tested with factors from 10 to 1000) or by stacking over a longer durations (> 90 days). This is generally consistent with the concept of convergence of the NCFs with stacking over time [e.g., *Sabra et al.*, 2005a; *Bensen et al.*, 2007; *Seats et al.*, 2012].

The source-receiver geometries under which accurate velocities can be obtained from the NCF techniques span a large range of length scales. Receiver array scales vary from dozens of meters [e.g., *deRidder and Dellinger*, 2011; *Young et al.*, 2011] to thousands of kilometers [e.g., *Lin et al.*, 2008; *Bensen et al.*, 2008, 2009]. In our set up, this suggests that configurations where L_s/L_x and Δ_{sx}/L_r ratios are large may be more representative of the Earth's ambient-noise source field. Although none of the idealized distributions are likely to be best representing the Earth's ambient field, we obtain the most accurate estimations when the sources are randomly distributed, or when they are randomly distributed on a shell.

One very critical part of testing this technique is the effect of the number of noise sources compared with the level of incoherent noise surrounding the receiver array. We vary the number of noise sources per time window from 1 to 2048, and the maximum amplitude of the incoherent noise from 10^{-6} to 10^{1} (Figure 7). We obtain more accurate estimates for simulations with more than ~16 noise sources per window (e.g., $N_s > 16$) and inaccurate estimates for simulations with fewer noise sources per window ($N_s < 16$). When the incoherent noise level is below ~1, the accuracy is sufficient to recover accurate attenuation. Within these two confines, there is little trade-off between these parameters for a wide range of dimensions values.

As with prior studies [e.g., *Yang and Ritzwoller*, 2008; *Cupillard and Capdeville,* 2010], our synthetic ambient field seismograms yield NCFs that contain appropriate amplitude information (e.g., Figures 3 and 4). We investigated the accuracy to which those amplitudes are retrieved with respect to frequency and the scale-lengths for the different source distribution configurations (Figure 6). In general, the NCFs calculated with equation 14 do not exhibit much difference from an attenuated Bessel function, which disagrees with analytical results of *Tsai* [2011] and *Weaver* [2011]. Within the confines of the parameter space described earlier, these simulations yield a better fit to an attenuated Bessel function.

While the azimuths of highest ambient noise energy may tend towards a coast or a seasonal variation in wave height for a short duration, no study has shown that an NCF stacked from many (e.g., >12) months of data can be described by a single localized source. The origin of the ambient seismic field sources is still unresolved. This likely comes from the complexity of the spatial and temporal distribution of noise sources and their respective contribution to the ambient seismic field spectrum [*Longuet-Higgins,* 1950; *Webb and Constable,* 1986; *Cessaro*, 1994; *Chevrot et al.,* 2007; *Kedar et al.,* 2007; *Ardhuin et al.*, 2011]. Furthermore, *Seats et al.*, [2012] demonstrated that coherency stacks from more overlapping short time windows (30min-1hour long rather than day-long) yields better source distributions than those from longer time windows. This can result from a better averaging process where large-magnitude sources do not dominate over the other sources recorded in successive time windows.

Ultimately, a combination of the proposed source configuration is more plausible than any individual one. We therefore created case that evenly draws from the four source scenarios shown in Figure 1. This combined source distribution provides results similar to that of the uniformly random (shell) distribution (Figure 8), where the phase velocity and attenuation results are reliable for a broad range of parameters. The take-home message from the combined scenario is that once sources are sufficiently distributed in both azimuth and distance from the receiver array, the phase and attenuation coefficients are resolved.

One major result from these simulations is that the unattenuated Bessel function fits best to NCF synthetics calculated with two or fewer sources per time window ($N_s \leq 2$). This is particularly true for nearly symmetric far-field distributions (i.e. circular and uniform sphere). Since we tested those cases for long durations of stacking (>4years), we cannot explain this result by simply stating the lack of sources. It is noteworthy that NCFs created from one to two sources per time window are inherently different from NCFs generated with 3 or more. In point of fact, it may be that those created with only two sources are largely dominated by a single source, and that NCFs generated with a single source per time window are different from those with multiple sources. Note that if $N_\mathbf{s}$ = 1, equation 14 may simplify to a more simple solutions. However, rather than converging to an augmented attenuation decay [e.g., *Tsai* 2011], the additional decay appears to cancel out such that there is virtually no attenuation [e.g., *Weaver* 2011]. Theoretical analysis where $N_\mathbf{s}$=1 (e.g., equations 12 and 13) suggests the stacked coherency to be independent of attenuation. Our results are then in good agreement with both the analytic work of *Weaver* [2011] and the empirical work of *Prieto et al.* [2009] and *Lawrence and Prieto* [2011].

It is precisely the fact that the coherency normalizes each record (and not each source) that makes the NCF sensitive to attenuation. Figure 9 illustrates the difference between comparing normalized records and comparing normalized sources. If each source is normalized for each receiver, then there is no measurable geometric spreading or attenuation, which agrees with *Weaver* [2011]. The plane wave formulation requires no geometric spreading, which should behave similar to the point source where each source is independently normalized for each receiver. A point source within an elastic medium should yield different amplitudes for each source-receiver pair as predicted by the geometric spreading inherent to the Bessel function formulation. Without appropriate normalization, the real coherency amplitudes would not decrease with distance similarly to a Bessel function. The additional amplitude decay caused by attenuation yields only increased waveform dissimilarity, which accounts for the reduced coherency amplitudes at greater distance.

It is also important to demonstrate that estimated attenuation coefficient are sensitive to the structure near the receivers, not near the sources or the path between sources and the receiver array. Therefore we test the effects due to attenuation variation at or near the sources. We compare the attenuation coefficients measured from the synthetic NCF stacks calculated with differing input attenuation coefficients for the regions near the receivers and near the sources. In the first case we set attenuation coefficients to zero for a 200km radius region surrounding the receivers, while maintaining the same attenuation coefficients for the source region as above, and opposite in the second case. We perform this test only for the uniform shell scenario with small source offset ($\Delta_{\mathbf{sx}}$=100) and intermediate-to-large source length ($L_{\mathbf{s}}$=1000) in order to separate the sources and receivers. This simple test confirms that the method measures attenuation near the receivers, and no attenuation near the sources, as illustrated in Figure 10.

Future analyses with the method of *Prieto et al*. [2009] might benefit from considering additional biases not addressed here. For example, 3D focusing effects bias amplitudes significantly within a heterogeneous medium [e.g., *Lin et al*., 2011]. *Prieto et al*. [2009] and *Lawrence and Prieto* [2011] attempted to reduce the focusing and defocusing effects by azimuthally averaging over large arrays (and all directions). However this averaging does not reduce all amplification effects for most 3D structures heterogeneous structures. Accounting for amplification with adjoint or finite frequency kernels for amplitude may help reduce such biases. Similarly, repeating the analyses conducted here with full 3D elastic [e.g., *Stehly et al*., 2011; *Cupillard et al*., 2012] wave propagation with intrinsic attenuation decay may illuminate potential biases in attenuation estimates due to structures between the sources and receivers.

While the results of this study support the link between the empirical interpretations of NCF energy decay as intrinsic seismic attenuation, there remains a lack of any analytical proof linking the increased amplitude decay to the functional form $e^{-\alpha(\omega)r_{xy}}$. Nevertheless, our simulations indicate that the functional form holds for a large variety of source-receiver configurations. Furthermore, the functional form is the intuitive solution. For an elastic medium, it is accepted that a well-constructed NCF represents an approximation of the Green's function between a given receiver pair, as if one receiver were a virtual source and the other were a virtual receiver (and visa versa for the negative time lag portion) [*Weaver and Lobkis*, 2004]. A Green's function including attenuation should be modified by a $e^{-\alpha(\omega) r_{xy}}$ term.

Conclusion:

This study numerically demonstrates that the *Prieto et al.*, [2009] method of measuring seismic attenuation from stacked ambient noise correlation functions is viable. These results are in contrast to analytical results in the literature, which may suggest that 1) assuming a "white homogeneous ambient source field" (or equipartition) is not equivalent to whitening the recorded ambient field, 2) correlating multiple sources is distinct from independently correlating each source, and 3) incoherent noise between the sensors may contribute to the NCF distance dependant decay. Our numerical results illustrate that attenuation coefficients are recoverable for a wide range of appropriate source conditions. These conditions include 1) a reasonable azimuthal distribution of sources (mostly outside the receiver array), 2) multiple sources recorded per time window, 3) many time windows to stack and 4) a receiver distribution providing ample station-to-station azimuths and station separations. For a variety of source conditions (including those with non-uniform source distributions) the phase velocity and attenuation are well recovered from synthetic NCFs. However, when we include fewer sources per time window ($N_s \leq 2$) in the simulations, the estimated attenuation coefficients are negligible, which corresponds to the analytical assessment of *Weaver* [2011] that single-source NCFs are independent from attenuation. With more sources per time window (e.g., N_s=128), the NCFs are only sensitive to the attenuation in the region of the receiver array.

Acknowledgements:

We thank the reviewers (in advance) for their comments and suggestions. This research was funded in part by NSF grant EAR 1050669.

References:

Aki, K., and B. Chouet (1975), Origin of coda waves: Source, attenuation, and scattering effects, J. Geophys. Res., 80, 3322–3342.

Ardhuin, F.; Stutzmann, E.; Schimmel, M.; Mangeney, A. (2011), "Ocean wave sources of seismic noise", *J. Geophys. Res.* **115**, C09004, doi:10.1029/2011JC006952.

Bensen, G.D., M.H. Ritzwoller, M.P. Barmin, A.L. Levshin, F. Lin, M.P. Moschetti, N.M. Shapiro, and Y. Yang (2007) Processing seismic ambient noise data to obtain reliable broad-band surface wave dispersion measurements, *Geophys. J. Int.*, 169, 1239-1260, doi: 10.1111/j.1365-246X.2007.03374.x, 2007.

Bensen, G.D., M.H. Ritzwoller, and N.M. Shapiro, Broad-band ambient noise surface wave tomography across the United States, *J. Geophys. Res.*, 113, B05306, 21 pages, doi:10.1029/2007JB005248, 2008.

Bensen, G.D., M.H. Ritzwoller, and Y. Yang (2009) A 3D shear velocity model of the crust and uppermost mantle beneath the United States from ambient seismic noise, *Geophys. J. Int.*, 177(3), 1177-1196.

Cessaro, R. K. (1994), Sources of primary and secondary microseisms, *Bull. Seismol. Soc. Am.*, 84, 142–148.

Chevrot, S., M. Sylvander, S. Benahmed, C. Ponsolles, J. M. Lefèvre, and D. Paradis (2007), Source locations on secondary microseisms in western Europe: Evidence for both coastal and pelagic sources, J. Geophys. Res., 112, B11301, doi:10.1029/2007JB005059.

Colin de Verdière, Y., (2006*a*) Mathematical models for passive imaging I: General background: Mathematical Physics, accessed 18August 18 2008; http://fr.arxiv.org/abs/math-ph/0610043.

Colin de Verdière, Y., (2006*b*) Mathematical models for passive imaging II: Effective Hamiltonians associated to surface waves: Mathematical Physics, accessed 18 August 18 2008; http://fr.arxiv.org/abs/math-ph/0610043.

Colin de Verdière, Y., (2009) Semiclassical analysis and passive imaging, *Nonlinearity* 22, R45–R75, doi:10.1088/0951-7715/22/6/R01.

Cupillard, P. and Y. Capdeville (2010), On the amplitude of surface waves obtained by noise correlation and the capability to recover the attenuation : a numerical approach. *Geophys. J. Int.*, Vol. 181, p. 1687-1700, doi:10.1111/j.1365-246X.2010.04586.x.

Cupillard, P., Y. Capdeville, L. Stehly and J.-P. Montagner (2012) Spectral element simulation of waveforms obtained by correlation of ambient seismic noise, in prep.

de Ridder, S. & Dellinger, J., 2011. Ambient seismic noise eikonal tomography for near-surface imaging at Valhall, *Leading Edge,* **30,** 506–512, doi:10.1190/1.3589108.

Derode, A., E. Larose, M. Campillo, and M. Fink (2003a) How to estimate the Green's function of a heterogeneous medium between two passive sensors? Application to acoustic waves, Appl. Phys. Lett., 83, 3054–3056.

Derode, A., E. Larose, M. Tanter, J. de Rosny, A. Tourim, M. Campillo, and M. Fink (2003b) Recovering the Green's function from field-field correlations in an open scattering medium, J. Acoust. Soc. Am., 113, 2973–2976.

Ekström, G., G. A. Abers, and S. C. Webb (2009) Determination of surface-wave phase velocities across USArray from noise and Aki's spectral formulation, *Geophysical Research Letters*, *36*(18).

Gerstoft, P., P. M. Shearer, N. Harmon, and J. Zhang (2008) Global P, PP, and PKP wave microseisms observed from distant storms, *Geophys. Res. Lett.*, 35, doi: 100.1029/2008GL036111.

Gudmundsson, O., A. Khan, and P. Voss (2007) Rayleigh wave group-velocity of the Icelandic crust from correlation of ambient seismic noise, Geophys. Res. Lett., 34, L14314, doi:10.1029/2007GL030215.

Gutenberg, B. and C.F. Richter (1954) *Seismicity of the Earth and Associated Phenomena*, 2nd ed., Princeton, N.J., Princeton University Press.

Harmon, N., C. Rychert, and P. Gerstoft (2010), Distribution of noise sources for seismic interferometry, *Geophysical Journal International*, **183**, *3*, 1470-1484, doi:10.1111/j.1365-246X.2010.04802.x.

Hasselmann, K. (1963) "A statistical analysis of the generation of micro-seisms", *Rev. Geophys.* **1** (2): 177–210, doi:10.1029/RG001i002p00177

Kedar, S., M.S. Longuet-Higgins, F.W.N. Graham, R. Clayton, C. Jones (2008) The origin of deep ocean microseisms in the north Atlantic ocean, *Proc. Roy. Soc. Lond. A*: 1–35.

Koper, K. D., B. de Foy, and H. Benz (2009) Composition and variation of noise recorded at the Yellowknife seismic array,1991–2007, *J. Geophys. Res*., 114, B10310, doi:10.1029/2009JB006307.

Larose, E., A. Derode, D. Corennec, L. Margerin, and M. Campillo (2005) Passive retrieval of Rayleigh waves in disordered elastic media, Phys. Rev. E, 72, 046607, doi:10.113/PhysRevE.72.046607.

Lawrence, J.F. and G. Prieto (2011) Attenuation Tomography of the Western United States from Ambient Seismic Noise, J. Geophys. Res. 116, B06302, doi:10.1029/2010JB007836.

Lin, F., M.P. Moschetti, and M.H. Ritzwoller (2008) Surface wave tomography of the western United States from ambient seismic noise: Rayleigh and Love wave phase velocity maps, *Geophys. J. Int.*

Lin, F.C., M.H. Ritzwoller, and W. Shen (2011) On the reliability of attenuation measurements from ambient noise cross-correlations, *Geophys. Res. Letts.*, 38, L11303, doi:10.1029/2011GL047366.

Longuet-Higgins, M. S. (1950) "A theory of the origin of microseisms", *Phil. Trans. Roy. Soc. London A* **243** (857): 1–35, doi:10.1098/rsta.1950.0012.

Peterson, J. (1980) Preliminary observations of noise spectra at the SRO and ASRO stations, *Open-File Report, 80-99* US Geological Survey, Albuquerque, NM.

Peterson, J. (1993) Observations and modeling of seismic background noise, *Open-File Report, 93-322,* US Geological Survey, Albuquerque, NM*.*

Prieto, G. A., and G. C. Beroza (2008) Earthquake ground motion prediction using the ambient seismic field, *Geophysical Research Letters*, *35*(L14304).

Prieto, G. A., J. F. Lawrence, and G. C. Beroza (2009) Anelastic Earth structure from the coherency of the ambient seismic field, *Journal of Geophysical Research 114*(B07303).

Prieto, G. A.. M. Denolle, J. F. Lawrence, G. C. Beroza (2011) On amplitude information carried by the ambient seismic field. *Comptes rendus geoscience. Thematic Issue: Imaging and Monitoring with Seismic Noise.* 343, 600-614.

Rhie, J. and B. Romanowicz, (2004), "Excitation of Earth's continuous free oscillations by atmosphere-ocean-seafloor coupling", *Nature* **431** (7008): 552–556, doi:10.1038/nature02942, PMID 15457256.

Rhie, J., and B. Romanowicz (2006) A study of the relation between ocean storms and the Earth's hum, Geochem. Geophys. Geosyst., 7, Q10004, doi:10.1029/2006GC001274.

Sabra, K. G., P. Roux, and W. A. Kuperman (2005a), Emergence rate of the time-domain Green's function from the ambient noise cross-correlation function, *J. Acoust. Soc. Am.*, *96*(3), 1182-1191.

Sabra, K. G., P. Gerstoft, P. Roux, W. A. Kuperman, and M. C. Fehler (2005b) Surface wave tomography from microseisms in Southern California, *Geophysical Research Letters*, *32*(L14), 311.

Sánchez-Sesma, F. J., and M. Campillo (2006) Retrieval of the Green's function from cross correlation; the canonical elastic problems, *Bulletin of the Seismological Society of America*, *96*(3), 1182-1191.

Schulte-Pelkum, V., P. S. Earle, and F. L. Vernon (2004) Strong directivity of ocean-generated seismic noise, *Geochem. Geophys. Geosyst.*, 5, Q03004, doi:10.1029/2003GC000520.

Seats, K.J., J.F. Lawrence and G.A. Prieto (2012) Improved ambient noise correlation functions using Welch's method, Geophys. J. Int., 118, DOI: 10.1111/j.1365-246X.2011.05263.x.

Shapiro, N.M., Campillo, M., (2004) Emergence of broadband Rayleigh waves from correlations of the ambient seismic noise. Geophys. Res. Lett. 31, L07614.

Shapiro, N. M., M. Campillo, L. Stehly, and M. H. Ritzwoller (2005) High-Resolution surface-wave tomography from ambient seismic noise, *Science*, *307*, 1615-1618.

Shapiro, N. M., M. H. Ritzwoller, and G. D. Bensen (2006) Source location of the 26 sec microseism from cross correlations of ambient seismic noise, Geophys. Res. Lett., 33, L18310, doi:10.1029/2006GL027010.

Stehly, L., Campillo, M., Shapiro, N. (2006) A study of the seismic noise from its long range correlation properties. J. Geophys. Res. 111, B10306.

Stehly, L., Campillo, M., Shapiro, N.M., Fry, B., Boschi, L., (2009) Tomography of the alpine region from observations of seismic ambient noise. *Geophys. J. Int.*, 178, 338–350.

Stehly, L., P. Cupillard and B. Romanowicz (2011) Towards improving ambient noise tomography using simultaneously curvelet denoising filters and SEM simulations of seismic ambient noise. *C. R. Geoscience*, Vol. 343, p. 591-599, doi : 10.1016/j.crte.2011.03.005.

Stutzmann, E., M. Schimmel, G. Patau, and A. Maggi (2009) Global climate imprint on seismic noise, *Geochem. Geophys. Geosyst.,* 10, Q11004, doi:10.1029/2009GC002619.

Suda, N., K. Nawa, and Y. Fukao (1998) Earth's background free oscillations, *Science*, 279, 2089–2091.

Tanimoto, T. (2007) Excitation of microseisms, *Geophys. Res. Lett*., 34, L05308, doi:10.1029/2006GL029046.

Tanimoto, T., J. Um, K. Nishida, and N. Kobayashi (1998) Earth's continuous oscillations observed on seismically quiet days, *Geophys. Res. Lett*., 25, 1553–1556,

doi:10.1029/98GL01223.
Tanimoto, T., S. Ishimaru, and C. Alvizuri (2006) Seasonality in particle motion of microseisms, *Geophys. J. Int*., 166, 253–266.
Tsai, V. C. (2011) "Understanding the Amplitudes of Noise Correlation Measurements", *J. Geophys. Res*., 116, B09311, doi:10.1029/2011JB008483.
Wapenaar, K. (2004) Retrieving the elastodynamic Green's Function of an arbitrary inhomogeneous medium by cross-correlation. *Phys. Rev. Lett*. 93, 254301.
Wapenaar, K., Slob, E., Snieder, R., Dec 2006. Unified Green's function retrieval by cross correlation. *Phys. Rev. Lett*. 97 (23), 234301.
Weaver, R. L., and O. I. Lobkis (2001), On the emergence of the Green's function in the correlations of a diffuse field, *J. Acoust. Soc. Am*., 110, 3011–3017.
Weaver, R. L., and Lobkis, O. I. (2005), Fluctuations in diffuse field-field correlations and the emergence of the Green's function in open systems. J. Acoust. Soc. Am., 117(6), 3432–3439.
Weaver, R. L., and O. I. Lobkis (2004), Diffuse fields in open systems and the emergence of the Green's function, *J. Acoust. Soc. Am*., 116, 2731–2734.
Weaver, R. L. (2011) On the amplitudes of ambient noise correlations and the inference of attenuation, *EOS Trans. AGU*, Fall Meeting.
Weemstra, C., A. Goertz, and L. Boschi (2011a) Towards a method for attenuation inversion from reservoir-scale ambient noise OBS recordings, *SEG Expanded Abstracts*, 30, 1592, doi:10.1190/1.3627507.
Weemstra, C., A. Goertz, and L. Boschi (2011b) Constraining attenuation with ambient noise correlations of reservoir scale seismic data, *EOS Trans. AGU*, Fall Meeting.
Yang Y., D.W. Forsyth (2008), Attenuation in the upper mantle beneath Southern California: Physical state of the lithosphere and asthenosphere, *J. Geophys. Res.*, *113*(B03308).
Yang, Y., and M. H. Ritzwoller (2008), Characteristics of ambient seismic noise as a source for surface wave tomography, *Geochem. Geophys. Geosyst*., 9, Q02008, doi:10.1029/2007GC001814.
Yao, H., R.D. van der Hilst, and M. Van de Hoop (2006) Surface-wave array tomography in SE Tibet from ambient seismic noise and two-station analysis I. Phase velocity maps, *Geophys. J. Int.*, *166*, 732--744.
Yao, H. and Van der Hilst, R.D. (2009) Analysis of ambient noise energy distribution and phase velocity bias in ambient noise tomography, with application to SE Tibet, *Geophys. J. Int.*, 10.1111/j.1365-246X.2009.04329.x
Young, M. K., N. Rawlinson, P. Arroucau, A. M. Reading, and H. Tkalčić (2011), High-frequency ambient noise tomography of southeast Australia: New constraints on Tasmania's tectonic past, *Geophys. Res. Lett.*, 38, L13313, doi:10.1029/2011GL047971.
Zhang, J., P. Gerstoft, and P. M. Shearer (2009) High-frequency P-wave seismic noise driven by ocean winds, *Geophys. Res. Lett.*, 36, doi: 1029/2009GL037761.
Zheng, S., X. Sun, X. Song, Y. Yang, and M. H. Ritzwoller (2008), Surface wave tomography of China from ambient seismic noise correlation, *Geochemistry Geophysics Geosystems*, *9*(Q05020).

Table 1: Description of Synthetic Scenarios

Source Array Geometry*	N_s/1800s	*Days*	*Overlap*	L_x (km)	L_s (km)	Δ_{sx} (km)	M_s
A (151 runs)	25	30	50%	100	10^1-10^4	10^1-10^4	2
B (151 runs)	25	30	50%	100	10^1-10^4	10^1-10^4	2
C (151 runs)	25	30	50%	100	10^1-10^4	10^1-10^4	2
D (151 runs)	25	30	50%	100	10^1-10^4	10^1-10^4	2
B (24 runs)	2^{0-8}	30	50%	100	10^3	5×10^2	1,2,4,8
B (24 runs)	2^{0-4}	365	50%	100	10^3	5×10^2	1,2,4,8

* The labels correspond to the sub-panels (A-D) in figure 1. A is a circle source. B is a linear source. C is a uniformly random filled circle. D is a uniformly random filled circular shell.

Figure 1

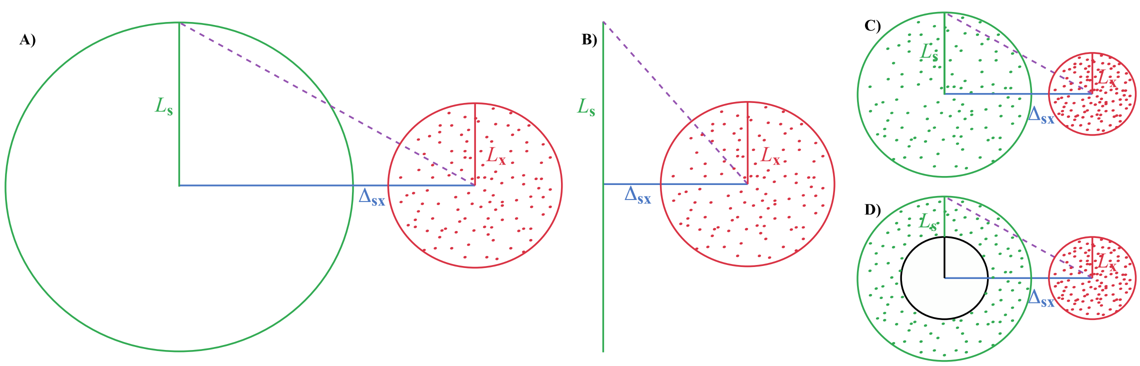

Figure 1: This figure illustrates the geometries we test, and the geometrical parameters. The source distribution (green) has a scale length (radius or half length) of L_s. The receiver distribution (red) has a scale length (radius) of L_x. The distance between the source center and the receiver center is given by Δ_{sx} (blue). The tangent of (L_s / Δ_{sx}) provides an approximate measure of single-hemisphere azimuthal range of the sources relative to the center of the array. The source distributions are referred to in the text as A) circular, B) linear, C) randomly uniform, and D) randomly uniform shell.

Figure 2

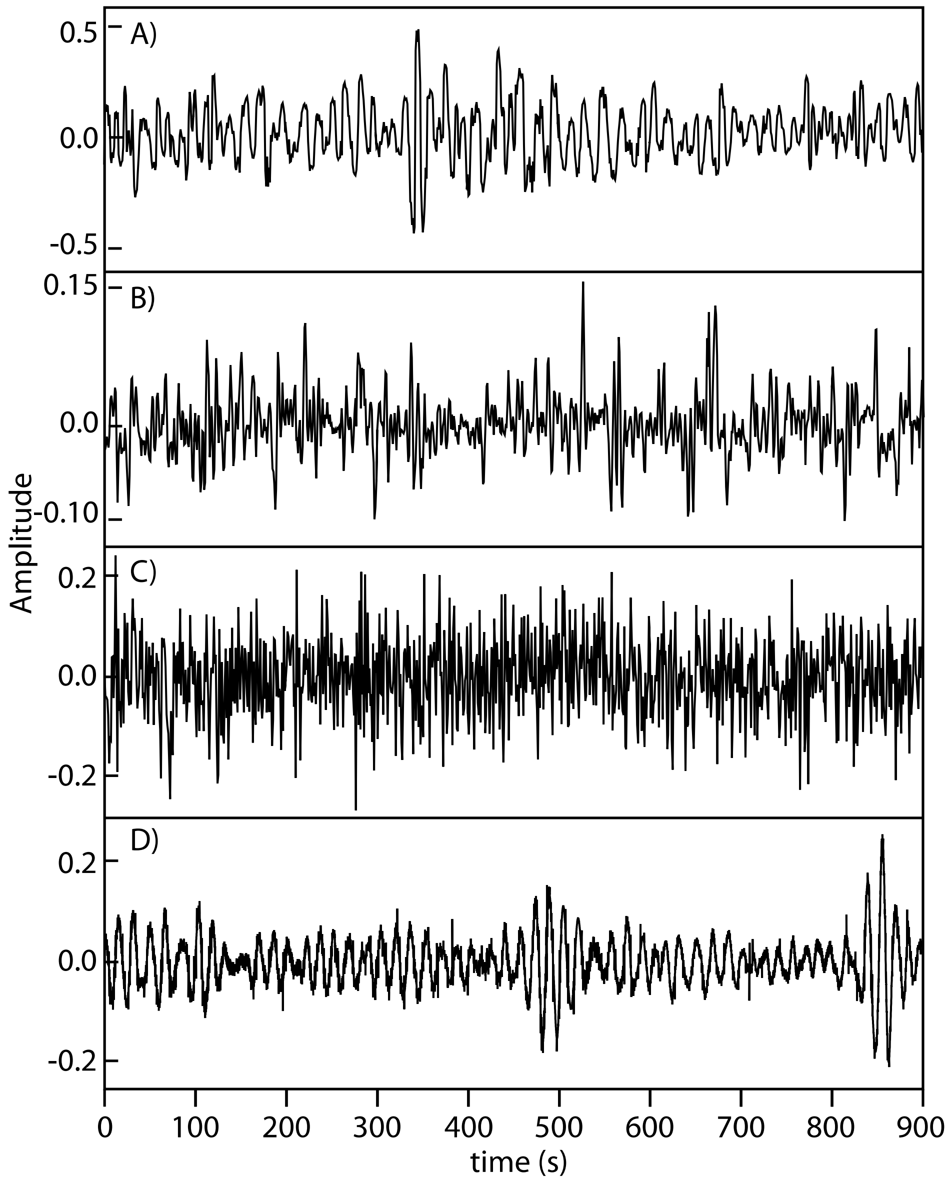

Figure 2: This figure illustrates three ambient seismograms generated using a stochastic set of sources with random source amplitudes and source geometries: A) circular source, B) linear source, C) uniformly random source, and D) Uniformly random source shell as shown in Figure 1. The same sensor location was used in each synthetic seismogram. The source length was L_s=2000 in each case and the source-receiver offset was Δ_{rs}=0 in each case. The number of sources used to generate this window was N_s = 128. The reduced high-frequency amplitudes in seismograms A) and D) are caused by greater attenuation accrued over a greater minimum distance between the sources and receivers.

Figure 3

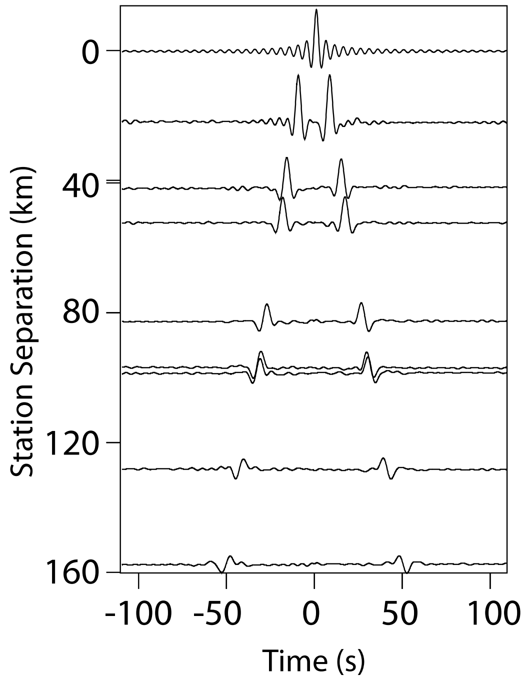

Figure 3: The noise correlation functions, bandpass filtered between 0.02 and 0.2 Hz, for a subset of synthetic seismograms generated using equation 14, a uniformly random source location distribution with source length L_s=2000 (panel C of Figure 1), source-receiver separation Δ_{rs}=0, and stacked for coherencies of 1800 s time windows over 90 days with 128 sources per time window.

Figure 4:

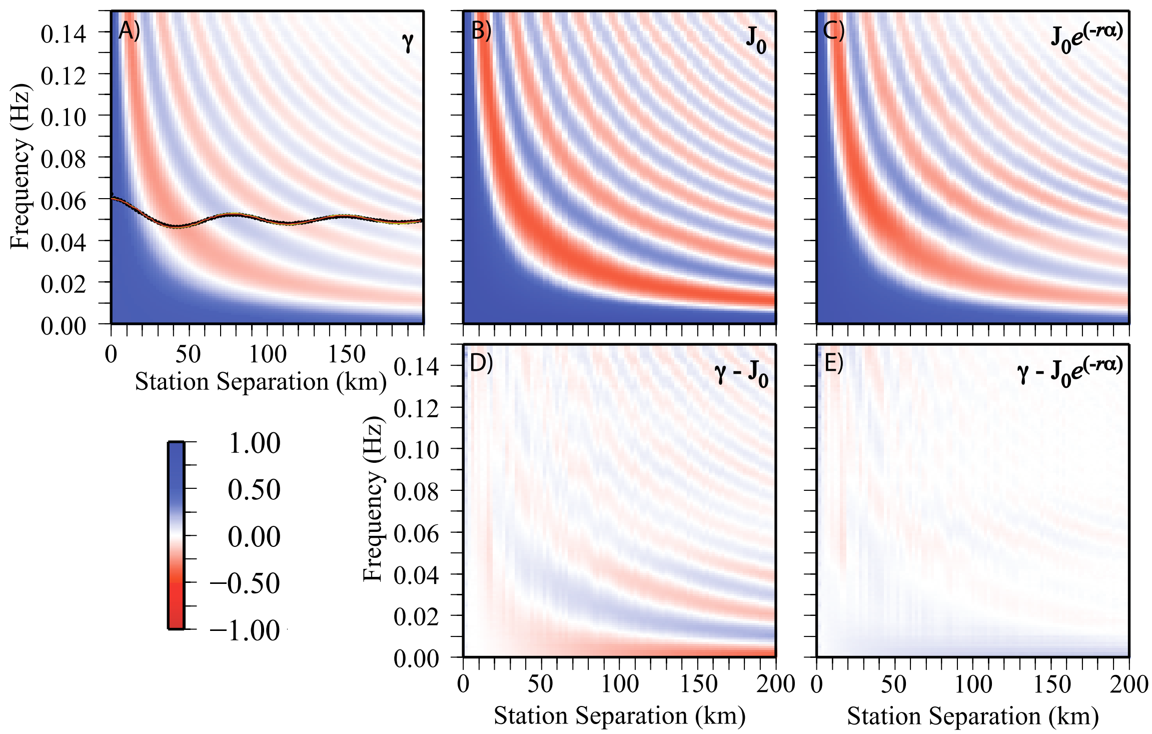

Figure 4: A) The real portion of the stacked coherencies, Re[$\gamma_{xy}(\omega)$], calculated in equation 14 for a uniformly random source location distribution with source length L_s=2000 (panel C of Figure 1), source-receiver separation Δ_{rs}=0, and stacked for coherencies of 1800s time windows over 90 days with 128 sources per time window. Each coherency is stacked according to station separation at 2km intervals. The real coherency values of are similar to B) the theoretical Bessel function, but better match the amplitudes of the C) attenuated Bessel function. The final panels illustrate the misfit between the observed real coherency measured from the synthetics as compared to the D) Bessel function and E) attenuated Bessel function.

Figure 5:

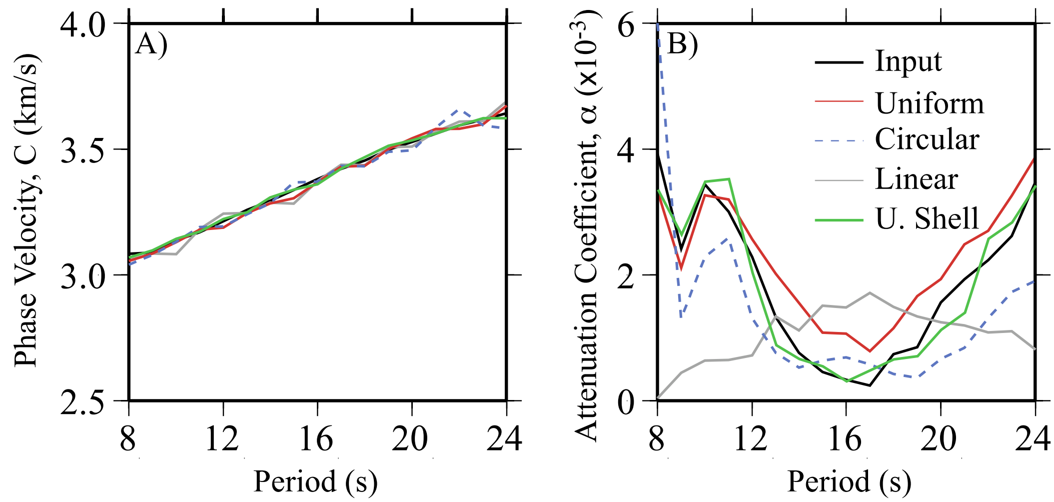

Figure 5: The A) phase velocity and B) attenuation coefficients input into the synthetic calculation (black) are recovered with differing degrees for the (red) uniformly random, (blue) circular, and (grey) linear source distributions. The attenuation measurements are not as accurate as the phase velocity estimates, but for the rough values are recovered. These curves are calculated using source location distributions with source length L_s=2000 (panel C of Figure 1), source-receiver separation Δ_{rs}=0, and stacked for coherencies of 1800s time windows over 90 days with 128 sources per time window. Each coherency is stacked according to station separation at 2km intervals (as in Figure 4) and fit with a 3-stage grid search.

Figure 6:

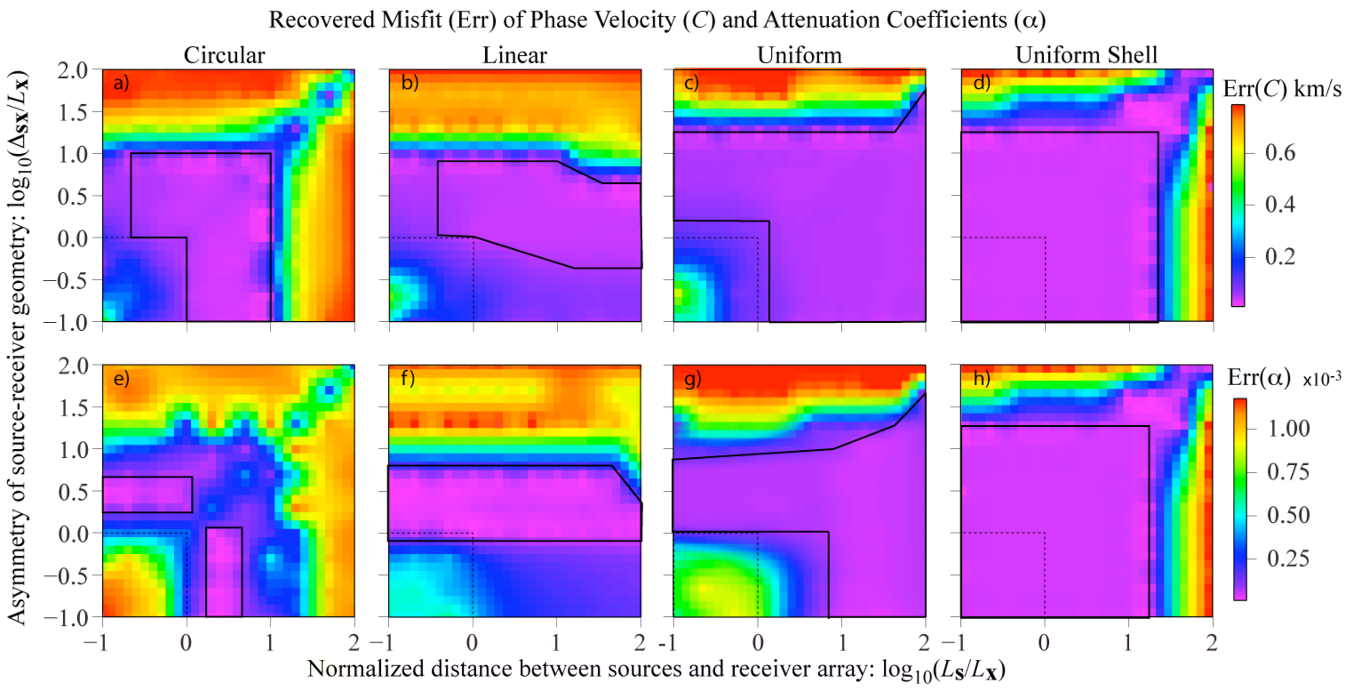

Figure 6: The RMS misfits for (a-d) phase velocity and (e-h) attenuation coefficients for simulations run with various length scales, source length L_s, receiver length L_x, and source-receiver separation Δ_{sx}. As expected, when L_s and Δ_{sx} are small compared to L_x (i.e. the sources are within the array – dotted box), the phase velocity and attenuation are not well recovered. This is also the case when the sources are over an order of magnitude more distant from the receivers than the receivers are from each other. The parameter-space of best fit lies within the bold black lines. These NCF stacks were calculated for coherencies of 1800s time windows over 90 days with 128 sources per time window. Note: panels (a-d) and (e-f) correspond to the geometries illustrated in panels (a-d) in Figure 1.

Figure 7

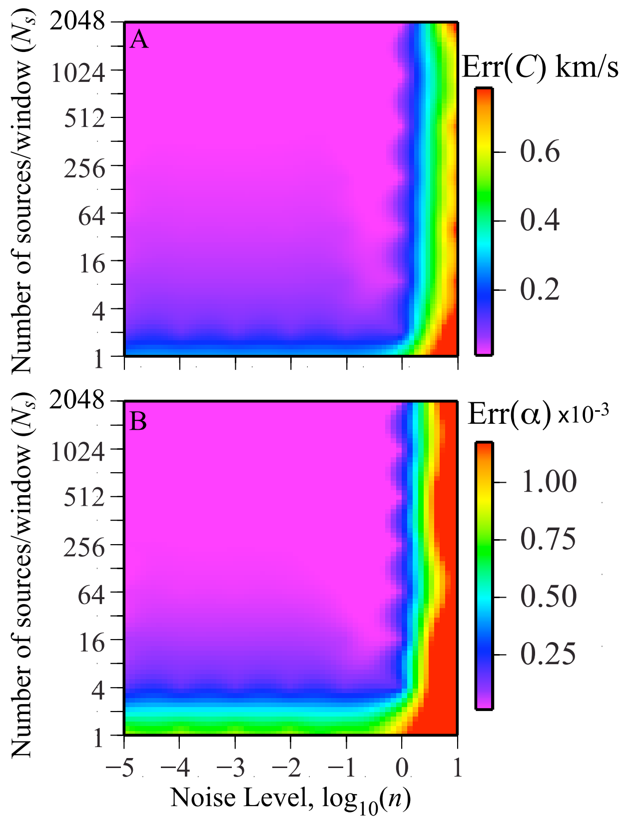

Figure 7: This figure illustrates the misfit tradeoff between the number of sources per window (N_s) and the maximum level of uniform incoherent white noise, n_{max}, at each receiver. The colors illustrate the misfit between the estimated and known input values for A) phase velocity, $C(\omega)$, and B) attenuation coefficients, α. The misfit is consistently low for $N_S > 16$ and $n_{max} < 1$. The misfits are calculated for simulations having uniformly random sources and receivers with geometric parameters L_s=1000, Δ_{sx}=100 and L_x=100, where the NCFs were stacked for coherencies of 1800s time windows over 90 days.

Figure 8

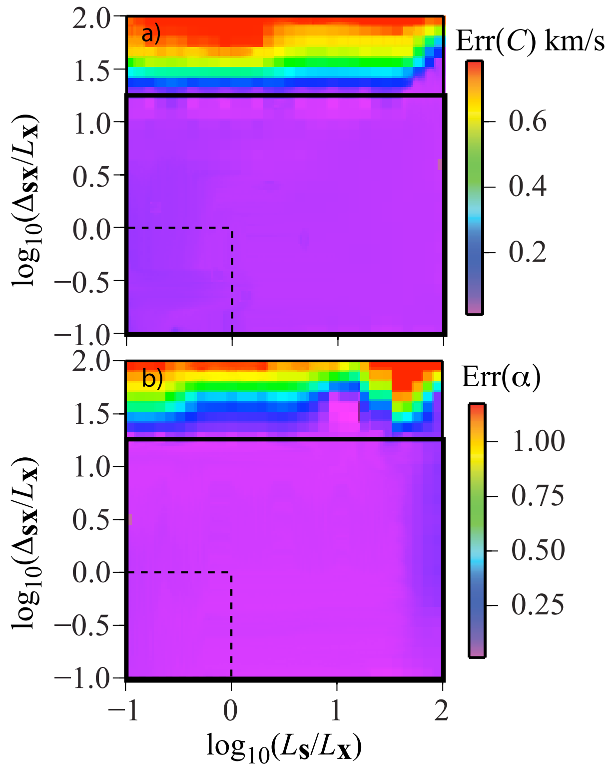

Figure 8: Similar to Figure 6 except, illustrating misfit between known and measured a) phase velocity, and b) attenuation coefficient for a single set of source distributions generated as a random amalgamation of the four source types illustrated in Figure 1.

Figure 9

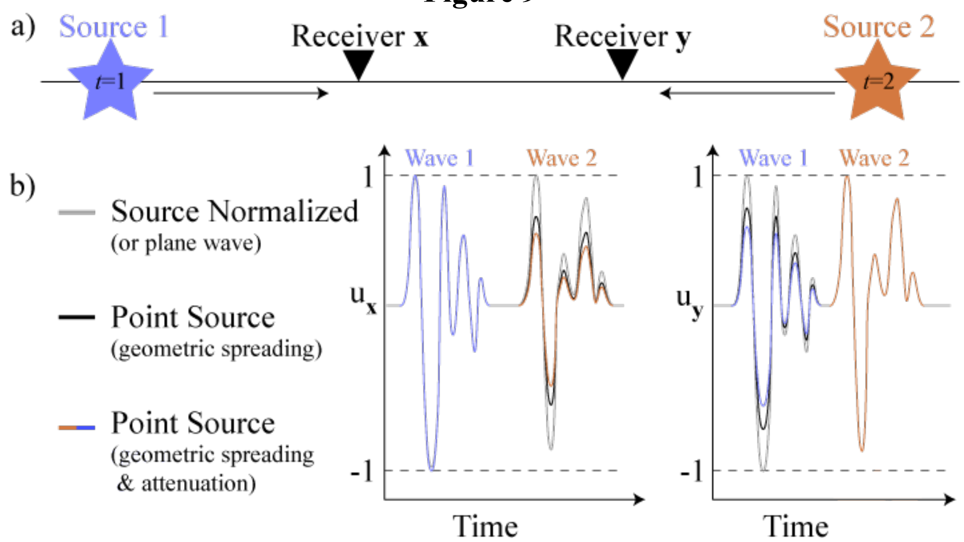

Figure 9: This cartoon represents the normalized seismic records for a) two sources (1 and 2) that occur at distinct times (*t*=1 & *t*=2), observed at two receivers (**x** and **y**). b) The seismic records at both receivers are most similar if the waves from each source-receiver pair are normalized separately (gray lines). Separate normalization for each source-receiver pair corresponds analytically to assuming purely elastic plane waves (no geometric spreading). Dissimilarity between seismograms at **x** and **y** occurs with the different travel times. Normalized records of waves propagating from two point sources through a purely elastic medium have dissimilar amplitudes at both receivers (black lines). The amplitudes vary more if the waves attenuate (blue and orange). Those dissimilarities accentuate with receiver separation.

Figure 9

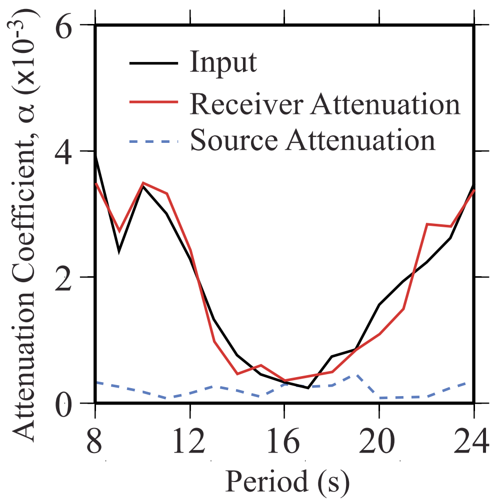

Figure 10: This figure illustrates the attenuation coefficients measured from synthetic NCF stacks calculated with (red) attenuation only in the 200km radius region containing the receivers, and (blue dashed) attenuation only outside the 200km radius region containing the receivers (i.e. source-side attenuation). The synthetics were calculated with a uniformly random shell source distribution, where the source offset and length scales are given by L_s=1000 and Δ_{sx}=100, and the receiver length scale is L_x=100. The NCF stacks were calculated for coherencies of 1800s time windows over 90 days with 128 sources per time window and an input attenuation (black) from *Prieto et al*. [2009].